

This content has been downloaded from IOPscience. Please scroll down to see the full text.

Download details:

IP Address: 64.106.38.20

This content was downloaded on 29/04/2025 at 15:02

Please note that [terms and conditions apply](#).

You may also like:

[Extreme Wave Height Analysis in Natuna Sea Using Peak-Over Threshold Method](#)

Ismail Abdul Jabbar and Nining Sari Ningsih

[Study on Fundamental Force of Extreme Wave on Complex Deepwater Jacket](#)

Jianjun Yi, Guoliang Zou and Pingshan Qin

[Global-scale changes to extreme ocean wave events due to anthropogenic warming](#)

Joao Morim, Sean Vitousek, Mark Hemer et al.

[Numerical prediction of Normal and Extreme Waves at Fukushima Offshore Site](#)

Atsushi Yamaguchi and Takeshi Ishihara

[Extreme wave height analysis using Weibull and Rayleigh distribution in some coastal areas affected by tsunami disasters and earthquakes in September 2018 at Central Sulawesi](#)

Y Mudin, H M D Labania, Abd Rahman et al.

Chapter 7

Ubiquitous nature of modulation instability: from periodic to localized perturbations

B Kibler, A Chabchoub, A Gelash, N Akhmediev and V E Zakharov

7.1 Introduction

Modulation instability (MI), also known as Benjamin–Feir instability, is considered to be the self-modulation of the continuous ‘envelope waves’ (i.e. regular wave trains in the context of deep water, or plane waves in optics) in the presence of small periodic or irregular noisy perturbations [1]. Since the 1960s, the propagation of weakly nonlinear dispersive wave packets affected by MI has been theoretically studied and experimentally observed in various fields of physics such as water waves, plasmas, laser light, electrical lines and Bose–Einstein condensates [2–16]. Their dynamical evolution can be easily modeled using the one-dimensional focusing nonlinear Schrödinger (NLS) equation [1–5]. The resulting dynamics consists of an initial linear stage and a subsequent nonlinear stage. For the former, a simplistic linear stability analysis can be applied; the effect of modulation instability is the result of interaction between a strong carrier harmonic wave ω_0 and weak amplitude sidebands $\omega_0 \pm \Omega$, i.e. a degenerate four-wave mixing process. The linearization of the NLS equation allows us to identify the instability criterion for the wave system under study [9], whereby one can determine the frequency threshold and the initial growth rate of perturbations. A typical exponential growth of the sidebands during wave propagation depicts the amplification of the initial weak perturbation imposed on the harmonic wave. Such a linear approach of MI ceases to be valid as soon as the perturbation reaches a comparable size to the carrier wave. One may expect that the rapid amplification of the perturbation favors nonlinear four-wave mixing processes, thus extending the energy cascade towards higher-order sidebands. Indeed, the linear stage of MI precedes a more complex evolution of wave packets, usually associated with the emergence of highly localized wave structures, the so-called nonlinear stage of MI [17]. The latter has received renewed attention since exact pulsating solutions of the complete MI evolution have been linked to the dynamics of rogue waves [18–21].

To address the comprehensive MI problem, some exact solutions on finite background called breathers were derived during the 1970s and 80s [2, 22–27], as the NLS equation belongs to the remarkable class of integrable systems [4]. Such NLS breathers only derived for periodic initial modulations have provided, as a first step, a powerful framework for interpretation of a specific range of MI related dynamics that play a fundamental role in the theory of freak waves. The elementary solutions are the Akhmediev breather (AB) [2], which describes the simplest MI scenario with only one growth-return cycle evolved from a weak periodic perturbation, and the Peregrine breather (PB) [25], also known as the lowest-order rational solution to the NLS equation, which is the single-cycle limiting case of the AB with infinite period (i.e. the doubly localized breather). These restrictions can be overcome when one goes beyond the elementary instability by considering such first-order solutions as building blocks to construct higher-order solutions (i.e. nonlinear superpositions of breathers) to describe MI dynamics of more complex initial wave systems towards the irregular noisy perturbation. For instance, second-order AB solutions describe a higher-order MI namely, starting from five-wave systems [2]. A complete classification of the hierarchy of higher-order rational solutions of the NLS equation was reported in reference [28] by taking into account independent degrees of freedom associated with physical translations of component breathers.

Only recently, some unique features of these first- or higher-order periodic solutions have been confirmed experimentally for various nonlinear media [29–41]. Some works have confirmed that breather dynamics appear even with initial conditions that do not correspond to the mathematical ideal [29, 37, 42, 43]. As a result, such coherent structures may emerge locally in nonlinear wave systems driven by noise or chaotic states. In that configuration, interaction between many unstable modes takes place, so that rogue breather waves may appear intermittently or randomly in space and time with associated long-tailed statistics [19, 44–46]. Until recently, such characterization has remained a considerable challenge in optics. However, advanced pulse metrology techniques such as specially designed ‘time-microscope’ or ‘time-lens’ systems allow us now to analyze temporal ‘snapshots’ of the nonlinear propagation of ultrafast random light. Real-time optical measurements have characterized the spontaneous emergence of breathers from the unstable breakup of a continuous wave induced by low-amplitude noise [47]. Moreover, similar experiments have demonstrated the central role played by ‘breather-like’ structures such as the Peregrine soliton in the emergence of heavy-tailed statistics in integrable turbulence [48].

In order to describe the general physical picture of MI before going further into the problems of turbulence in integrable systems and rogue wave occurrence [49–51], one has to extend the MI analysis to *localized* weak perturbations of the plane wave, with a larger physical significance than periodic perturbations requiring the whole infinite space. To this end, a particular subset of higher-order breather solutions, known as superregular breathers, was recently derived [52, 53]. These solutions are defined as a nonlinear superposition of N pairs (where N is an integer) of quasi-Akhmediev breathers propagating in opposite directions. They can start with infinitesimally small localized perturbations and exhibit a combination of unique physical features in terms

of propagation behavior. In addition to the development of perturbation into special pairs of breathers, the reverse process is another important scenario, for which N -pairs of quasi-Akhmediev breathers are almost annihilated to a small localized perturbation as a result of their collision. Corresponding experimental confirmations were simultaneously reported in optics and hydrodynamics [54]. Such N -pair breather solutions are able to describe different configurations of the nonlinear stage of MI such as the amplification, annihilation, or even ghost-interaction of nearly any individual or ensemble of localized perturbations on a plane wave [52–54]. Recently, analogs of superregular breathers were found in the higher-order generalized NLS equation [55, 56], which demonstrates the general character of these solutions.

In this chapter, we consider the nonlinear stage of MI in the case of localized weak perturbations and, by using a unique mathematical formalism, we review the recent theoretical and experimental advances, more specifically, the dynamics of superregular breathers. Complementary numerical simulations of noise-driven MI are analyzed to give an advanced comprehensive approach of this ‘localized’ MI problem. In section 7.2, we provide the theoretical description for NLS superregular breathers. Section 7.3 is devoted to the description of the distinct experimental configurations for the sake of observation of such breather waves in optics and hydrodynamics. Section 7.4 presents some supplementary numerical studies of MI induced by time-localized noise that confirm predictions from the nonlinear wave theory. Finally, section 7.5 provides conclusions and an outlook on novel research directions.

7.2 Breather formalism

In the following, we use the breather formalism of reference [54] within the framework of the self-focusing NLS equation in dimensionless form that describes wave propagation in space:

$$i\psi_\xi + \frac{1}{2}\psi_{\tau\tau} + |\psi|^2\psi = 0. \quad (7.1)$$

Here, the subscripted variables stand for partial differentiations. The variable ψ denotes the wave envelope which is a function of ξ (a scaled propagation distance or longitudinal variable) and τ (a co-moving time, or transverse variable, moving with the wave-group velocity). This equation usually describes the nonlinear wave evolution in various media, in particular, surface gravity waves in deep-water conditions and light waves in standard optical fibers for telecommunications.

We study the MI of the plane wave solution, written as $\psi_0 = Be^{iB^2\xi}$, where B is the finite amplitude of the plane wave. For simplicity, the latter amplitude of the background is scaled to 1. It is well-known that this solution is unstable with respect to small perturbations [9], with (angular) frequencies located within the range $0 < |\Omega| < 2$. The corresponding growth rate of instability, given by the linear stability analysis, is $\Gamma(\Omega) = \Omega(1 - \Omega^2/4)^{1/2}$. The maximum growth rate value $\Gamma = 1$ is reached for $\Omega = \pm\sqrt{2}$. In the presence of a background plane wave, the self-focusing NLS equation (7.1) has an exact N -breather solution, which can be constructed by the appropriate integration technique. This requires study of the auxiliary linear

Zakharov–Shabat system [27] with the complex spectral parameter $\lambda = \lambda_{\text{Re}} + i\lambda_{\text{Im}}$. The wave function solution of this system has a cut on the real axis where $-1 < \lambda_{\text{Re}} < 1$. Each breather adds a simple pole to the wave function at some point of λ -plane, including possibly the cut (i.e. Akhmediev breather solution). Coordinates of the pole in λ -plane describe the main breather properties (amplitude, group velocity, period of oscillation, etc). In the following, N -breather solutions were found using the dressing method as an integration technique; theoretical details can be found in references [52, 53, 57]. Note that the Jukowsky transform of the spectral parameter $\lambda = (\rho + \rho^{-1})/2$ with $\rho = R e^{i\alpha}$ was used [58]. This allows the mapping of the cut onto the circle of unit radius and λ -plane onto the outer part of this circle, so that the coordinates of the pole are described by the radial and angle coordinates R and α , as depicted in figure 7.1. Furthermore, each breather has two additional parameters μ and θ , which describe phase shifts in space and time and between different breathers.

The general one-breather solution has four real parameters R , α , μ , θ and can be described by the following expression [52–54, 59–61]:

$$\psi = \left(1 + 2 \left(R + \frac{1}{R} \right) \cos \alpha \frac{q_1^* q_2}{|q_1|^2 + |q_2|^2} \right) e^{i\xi}, \quad (7.2)$$

where

$$\begin{aligned} q_1 &= e^{-\phi} - \frac{e^{\phi-i\alpha}}{R}, & q_2 &= e^{\phi} - \frac{e^{-\phi-i\alpha}}{R}, \\ \phi &= \eta\tau + \gamma\xi + \frac{\mu}{2} + i \left(k\tau + \delta\xi - \frac{\theta}{2} \right), \\ \eta &= -\frac{1}{2} \left(R - \frac{1}{R} \right) \cos \alpha, & k &= -\frac{1}{2} \left(R + \frac{1}{R} \right) \sin \alpha, \\ \gamma &= -\frac{1}{4} \left(R^2 + \frac{1}{R^2} \right) \sin 2\alpha, & \delta &= \frac{1}{4} \left(R^2 - \frac{1}{R^2} \right) \cos 2\alpha. \end{aligned}$$

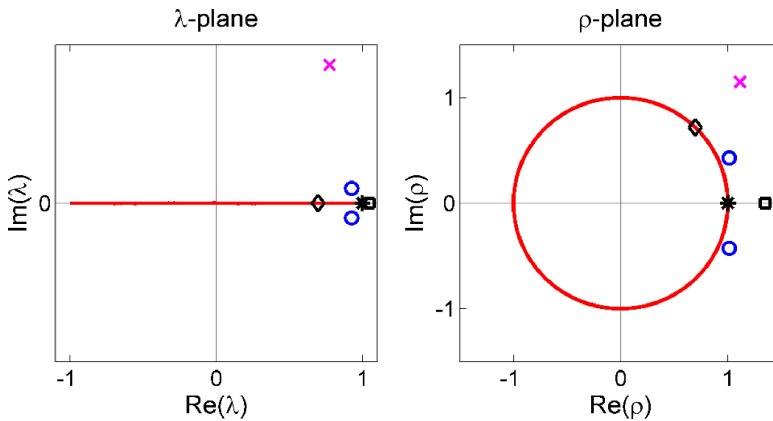


Figure 7.1. Application of the Jukowski transform to the plane of the complex spectral parameter λ . Poles of fundamental one-breather solutions are shown with markers: (\diamond) Akhmediev breather, (\square) Kuznetsov–Ma breather, (\square) Peregrine breather, (\circ) quasi-Akhmediev breather, (\times) general one-breather solution. The superregular one-pair solution is formed by the two quasi-AB with opposite group velocities (\circ - \circ).

The parameters R , α are the polar coordinates of the point in the ρ -plane (see figure 7.1, $R \geq 1$, $\frac{\pi}{2} > \alpha > -\frac{\pi}{2}$), and they control the main breather properties. In general, the one-breather solution is a localized object with characteristic size $\tau_0 = 1/((R - 1/R)\cos \alpha)$, moving on top of the continuous wave with group velocity $V_g = -\gamma/\eta = -\sin \alpha(R^4 + 1)/(R(R^2 - 1))$, and oscillating (in ξ variable) with period $T = 4\pi R^2/((R^4 - 1)\cos 2\alpha)$. Parameters R and α control the main breather properties, whereas μ , θ define the location as well as phase of the breather and vary in the range $[0, 2\pi]$. When $R = 1$, $\alpha \neq 0$, the solution is an Akhmediev breather (see figure 7.2(a)) that becomes the Peregrine soliton in the limit $\alpha \rightarrow 0$. For low values of V_g ($R \neq 1$, $\alpha \rightarrow 0$), we approach the limit of Kuznetsov–Ma breathers [62], whereas for high values of V_g and τ_0 ($R = 1 + \varepsilon$, where ε is a small parameter), we obtain the class of quasi-Akhmediev breathers (see figures 7.2(b) and (c)).

A general two-breather solution can be also obtained [52, 53]. It has four main parameters $R_{1,2}$, $\alpha_{1,2}$ and four additional phase-shift parameters $\mu_{1,2}$, $\theta_{1,2}$ (subscripts 1 and 2 correspond to the first and second breather). In the general N -breather solution, each i -th breather has similar four parameters R_i , α_i , μ_i , θ_i , so that the total solution is described by $4N$ parameters. The cut in the λ -plane allows construction of such a configuration of poles (when the poles are paired near the cut on the opposite sides) that the corresponding solution must be a small perturbation of the initial plane wave at the moment of breather collision. These solutions are referred to as superregular breathers. To construct the simplest one-pair superregular breather, the phases of the solution have to be the same at $\pm\infty$ by the τ coordinate at any fixed ξ , since a small perturbation of the plane wave background cannot change the phase of the whole solution at infinity. This happens when breathers move in opposite directions while $\alpha_1 = -\alpha_2 = \alpha$ (see figure 7.1). In the case $R_1 = R_2 = 1$, the solution is

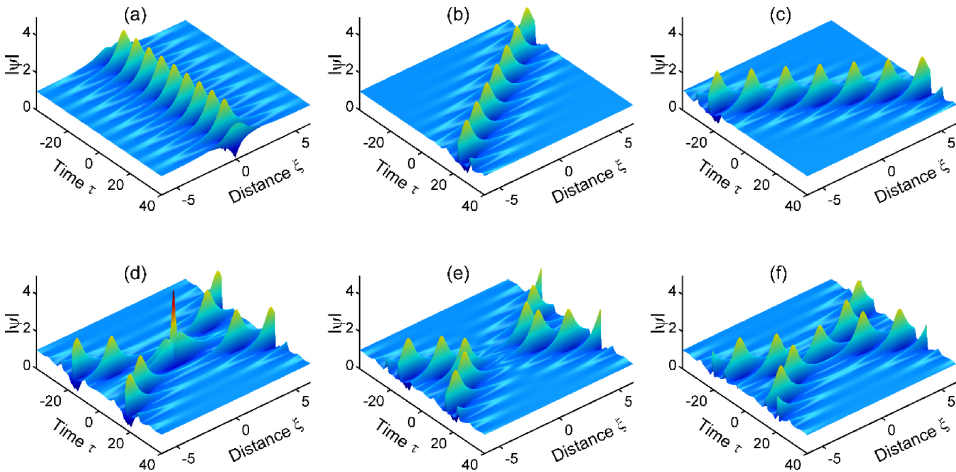


Figure 7.2. Examples of one-breather solutions and one-pair breather solutions. (a) Akhmediev breather ($R = 1$, $\alpha = 0.4$, $\theta = 0$, $\mu = 0$). (b) and (c) Quasi-Akhmediev breathers ($R = 1.1$, $\alpha = \pm 0.4$, $\theta = 0$, $\mu = 0$). (d)–(f) One-pair breather solution ($R = 1.1$, $\alpha = 0.4$) with the following phase shifts: $\theta_{1,2} = 0$, $\theta_{1,2} = \pi/2$, (superregular case), and $\theta_{1,2} = \pi$, respectively ($\mu_{1,2} = 0$ for all cases).

a pure plain wave (except the special case of degenerate breather solutions, which we do not discuss here), so that two Akhmediev breathers with opposite values of angular parameter completely annihilate each other. Consequently, when R_1 and R_2 are close to 1, two quasi-Akhmediev breathers almost annihilate at the moment of collision with the formation of a small perturbation of the plane wave. Thus, the amplitude of the perturbation is controlled by the difference of $R_{1,2}$ from the unity. The small parameter $\varepsilon = (R - 1)$ characterizes the amplitude of the perturbation at the moment of breather quasi-annihilation. In principle, quasi-annihilation can be observed at wide range of phase parameters $\mu_{1,2}$, $\theta_{1,2}$, however, the most effective annihilation occurs when $\theta_1 + \theta_2$ is close to π . Indeed, phase shifts affect the shape and the amplitude of the perturbation. The difference between $\theta_1 + \theta_2$ and π defines the degree of complexity of the wave profile at the area of collision. The solution is superregular when the phases are adjusted in a way that the perturbation is sufficiently small. The detailed description of the impact of parameters μ and θ can be found in references [52, 53], as well as some examples of complicated two and three-pair breather solutions and discussion of a general N -pair solution.

In the following, we study the simplest one-pair breather solution. It can be obtained from a general two-breather solution by setting $R_1 = R_2 = R = 1 + \varepsilon$, $\alpha_1 = -\alpha_2 = \alpha$, and can be written in the following form:

$$\psi = \left(1 + \left(R^2 - \frac{1}{R^2} \right) \frac{N}{\Delta} \sin 2\alpha \right) e^{i\xi} \quad (7.3)$$

$$\begin{aligned} N &= \left(R - \frac{1}{R} \right) \sin \alpha \left(|\mathbf{q}_1|^2 q_{21}^* q_{22} + |\mathbf{q}_2|^2 q_{11}^* q_{12} \right) \\ &\quad - i \left(R + \frac{1}{R} \right) \cos \alpha \left[(\mathbf{q}_1^* \cdot \mathbf{q}_2) q_{21}^* q_{12} - (\mathbf{q}_1 \cdot \mathbf{q}_2^*) q_{11}^* q_{22} \right], \\ \Delta &= \left(R + \frac{1}{R} \right)^2 \cos^2 \alpha |q_{11} q_{22} - q_{12} q_{21}|^2 \\ &\quad + \left(R - \frac{1}{R} \right)^2 |\mathbf{q}_1|^2 |\mathbf{q}_2|^2 \sin^2 \alpha, \end{aligned}$$

where $\mathbf{q}_i = (q_{i1}, q_{i2})$ is a two-component vector function, so that

$$\begin{aligned} q_{11} &= e^{-\phi_1} - \frac{e^{\phi_1 - i\alpha}}{R}, & q_{12} &= e^{\phi_1} - \frac{e^{-\phi_1 - i\alpha}}{R}, & q_{21} &= e^{-\phi_2} - \frac{e^{\phi_2 + i\alpha}}{R}, & q_{22} &= e^{\phi_2} - \frac{e^{-\phi_2 + i\alpha}}{R}, \\ \phi_1 &= \eta\tau + \gamma\xi + \frac{\mu_1}{2} + i \left(k\tau + \delta\xi - \frac{\theta_1}{2} \right), & \phi_2 &= \eta\tau - \gamma\xi + \frac{\mu_2}{2} - i \left(k\tau - \delta\xi + \frac{\theta_2}{2} \right), \end{aligned}$$

and the parameters η , k , γ , and δ are as defined previously.

Figures 7.2(d)–(f) show some particular arrangements of the just-discussed one-pair breather solution ($R = 1.1$, $\alpha = 0.4$) with the following values of phase shifts: $\theta_{1,2} = 0$, $\theta_{1,2} = \pi/2$, and $\theta_{1,2} = \pi$, respectively ($\mu_{1,2} = 0$ for all cases). The

synchronization of the collision is obtained for $\theta_{1,2} = 0$, thus leading to the formation of the high-amplitude peak at the origin ($\xi = 0, \tau = 0$) as shown in figure 7.2(d) [37, 60, 61]. Figure 7.2(e) shows the quasi-annihilation of breathers at the origin when $\theta_{1,2} = \pi/2$. This corresponds to a small localized perturbation of the continuous wave on the line $\xi = 0$ (superregular case) [51–53]. Another particular interaction is obtained for $\theta_{1,2} = \pi$ (see figure 7.2(f)). Then, the collision point is just another maximum of either breather solution. Each breather then appears seemingly without influence of the collision process; this particular case is here called a ghost-interaction of breathers. Quasi-Akhmediev breathers shown in figures 7.2(b) and (c) are neither periodic in time nor space. They are periodic along the line connecting the peak maxima given by the group velocity V_g (see figures 7.3(a) and (b)), and breathers propagate in opposite directions to infinity with a constant velocity before or after the collision area. Note that for the one-pair solution, shown in figures 7.2(d)–(f), there is only one collision point in the plane (ξ, τ).

In the following, we focus on the novel scenario of quasi-annihilation of breathers. When $\theta_1 + \theta_2$ is exactly equal to π (for example, $\theta_{1,2} = \pi/2$ in figure 7.2(e)), the quasi-annihilation is the most effective. In this case, at the moment of breather collision ($\xi \sim 0$), the perturbation $\delta\psi$ on the continuous wave (i.e. $\psi = 1 + \delta\psi$) can be approximated by the following formula:

$$\delta\psi \approx \frac{4i\epsilon \cosh(i\alpha - \xi \sin 2\alpha) \cos\left(2\tau \sin \alpha - \frac{\theta_1 - \theta_2}{2}\right)}{\cosh(2\epsilon\tau \cos \alpha)}. \quad (7.4)$$

The perturbation is localized in time and can contain many oscillations, but their number decreases by decreasing α . The number of oscillations also defines the main perturbation frequency of the wave envelope. Note that R and α also govern the

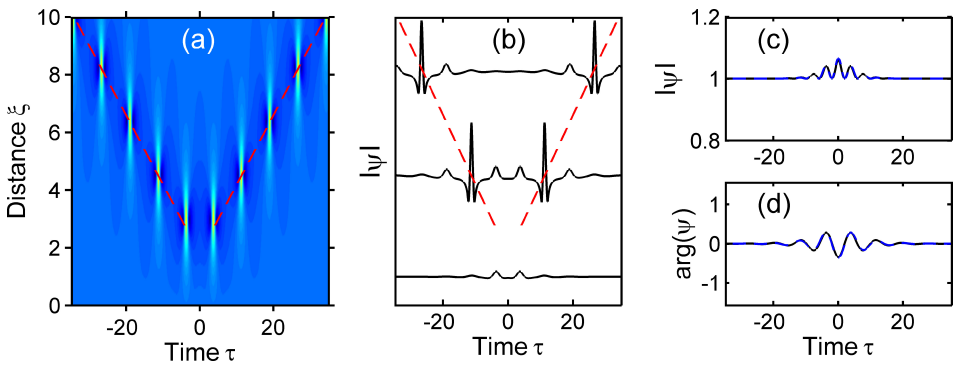


Figure 7.3. (a) Top view of figure 7.2(e), focused on the perturbation development into a pair of quasi-Akhmediev breathers propagating in opposite directions. Dashed red lines show the group velocity $V_g = \gamma/\eta$ calculated for each breather. (b) Corresponding amplitude profiles of the one-pair superregular breather at $\xi = 1, 4.5$, and 8.1 . (c) and (d) Amplitude and phase profiles of the approximated perturbation (blue dashed line) calculated with equation (7.4) and compared to the exact profile (black solid line) of the quasi-annihilated breathers at $\xi = 0$ observed in figure 7.2(e).

angle that separates quasi-AB trajectories in the plane (ξ, τ) . Moreover, the temporal width of the initial perturbation increases with decreasing ε , while its amplitude decreases. Figures 7.3(c) and (d) show the comparison between the approximated perturbation and the exact profile of the quasi-annihilated breathers at $\xi = 0$ from figure 7.2(e). We observe that the simplified approach of $\delta\psi$ gives an excellent fit of the small localized perturbation even here with $\varepsilon = 0.1$.

An initially small localized perturbation of the continuous wave grows at first exponentially. It is described by the well-known equations for the linear stage of modulation instability. It should be stressed that the Fourier spectrum of the superregular-type perturbations overlaps with the MI growth region $0 < |\Omega| < 2$. Similar to the Akhmediev breather solution (see, for instance reference [63]), the main frequency of superregular perturbation corresponds to the maximum of the MI growth rate ($\Omega_{\max} = \pm\sqrt{2}$) for $\alpha = \pi/4$, as illustrated in figure 7.4.

Then it develops into a pair of breathers propagating in opposite directions, as shown in figure 7.3. We note that such solutions leave after the propagation of breathers a continuous wave with a different phase (the difference with the phase at infinity is 4α) [53]. The perturbed part of the plane wave almost returns to the initial state, and this can be treated as a local Fermi–Pasta–Ulam (FPU) recurrence. Recall that the FPU recurrence is described by Akhmediev breathers for periodic perturbations and the presence of a similar phase shift [64]. Moreover, the pure homoclinic Akhmediev two-breather solution was studied in reference [53]. Namely, it was shown that when angular parameters of the solution are linked by $|\alpha_1| + |\alpha_2| = \pi/2$, the pure homoclinic (i.e. with zero phase shift) FPU recurrence occurs. This idea can be generalized to the multiple Akhmediev breather case and used to describe the complex periodic scenario of MI development leading to the FPU recurrence to exactly the same initial condition. To conclude this section, it is worth noting that the reverse process, implying the quasi-annihilation of a pair of quasi-Akhmediev breathers, is simply obtained by applying the time-reversal operation, which corresponds to $\theta_{1,2} = \frac{\pi}{2} + \pi$ (i.e. ξ becomes $-\xi$ in figures 7.2 and 7.3).

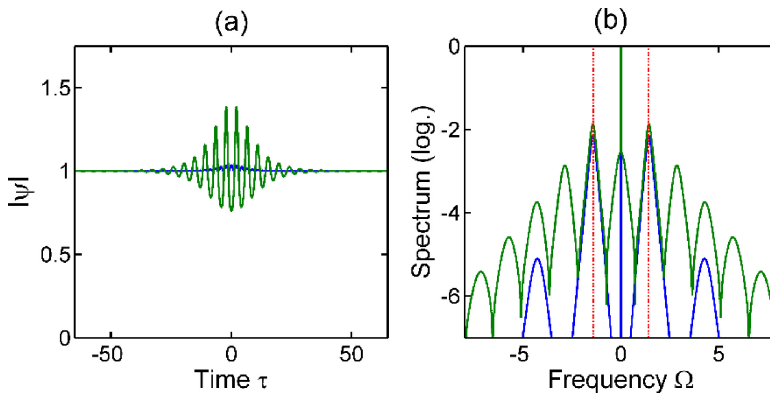


Figure 7.4. Modulation instability development for the one-pair superregular breather with $R = 1.1$ and $\alpha = \pi/4$. (a) Temporal profiles $|\psi(\tau)|$ at different propagation distances $\xi = 0$ (blue lines) and $\xi = 1$ (green lines). (b) Corresponding Fourier spectra $|\tilde{\psi}(\Omega)|$ in log scale. The dotted red lines indicate the positions of maximum MI growth rate Ω_{\max} and coincide with the positions of maximal amplitudes of the perturbation spectrum.

7.3 Experimental demonstrations

The current technical capability to manipulate light and water waves allows us to develop experimental setups to demonstrate the existence of superregular breathers in real nearly conservative physical systems [53], namely a water wave tank and an optical fiber workbench, as shown in figure 7.5. Such systems were specially designed to ensure as small a contribution as possible from higher-order effects beyond the second-order dispersion and the cubic nonlinearity. The parameters were chosen to highlight the creation and annihilation dynamics related to superregular breathers, as shown in figure 7.3. Note that a low value of the parameter α and considerable value of ε were chosen due to some technical restrictions of the experimental setups.

Each system is capable of synthesizing non-trivial wave profiles in the temporal domain according to equations (7.2) and (7.3). Such ideal excitation of the MI process is a prerequisite to exactly observe the dynamics shown in figure 7.3 instead of more complex behaviors [33]. As breather solutions are unstable waves, a non-ideal condition will induce the emergence of asymmetric wave profiles or/and introduce some complex spatial recurrence phenomena.

7.3.1 Water waves

In water wave experiments (see figure 7.5(a)), the initial wave profiles are generated with a single-flap paddle located at one end of a tank. An electric signal, calculated using the exact mathematical expression describing the water surface elevation, controls a hydraulic cylinder that drives the paddle to directly modulate the water surface height in the temporal domain. To this end, one has to fix the initial amplitude a_0 and the wavenumber of the carrier wave k_0 , thus defining the steepness $a_0 k_0$ of the quasi-regular wave train. We set the amplitude to be $a_0 = 0.01$ m and the wavenumber $k_0 = 10$ rad m⁻¹ while the water depth is 1 m to satisfy deep-water conditions. The frequency of the carrier wave is given by the dispersion relation of linear deep-water wave theory, $\omega_0 = (gk_0)^{\frac{1}{2}}$, where g is the gravitational acceleration. The surface elevation $\eta(z, t)$ is related to the NLS solution ψ to second order in steepness as follows:

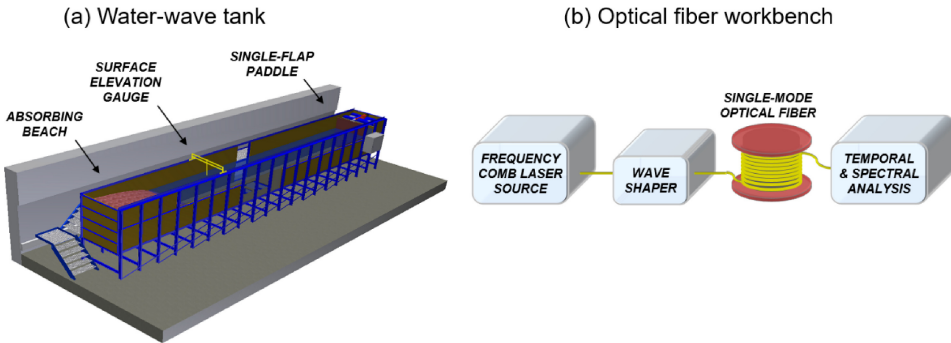


Figure 7.5. Experimental setups used to demonstrate the existence of superregular breather waves based on (a) a water wave tank and (b) an optical fiber workbench. (Adapted from [54].)

$$\eta(z, t) = \text{Re} \left\{ \psi(z, t) e^{i(k_0 z - \omega_0 t)} + \frac{1}{2} k_0 \psi^2(z, t) e^{2i(k_0 z - \omega_0 t)} \right\}. \quad (7.5)$$

The tank dimensions are 15 m \times 1.6 m \times 1.5 m. In order to avoid wave reflections in the wave flume, an absorbing beach is installed at the opposite end. To overcome the limited length of the wave flume, the propagation was split into several stages and we reconstructed the full wave dynamics afterwards. After starting the breather wave generation repetitively with different initial conditions given from theory, the wave profiles were measured at 4.5 and 9 m from the flap with wave gauges. Measurements at 9 m served as new initial conditions for the wave maker in the next stage of the experiments. This process was repeated four times to reach the propagation distance of 31.5 m.

The correspondence between the theory and experiment can be retrieved by recalling that dimensional distance z (m) and time t (s) are related to the previous rescaled variables by $z = \tau/(\sqrt{2} k_0^2 a_0) + c_g t$ and $t = 2\xi/(k_0^2 a_0^2 \omega_0)$, with $c_g = \omega_0/(2k_0)$. Using these latter relations and inverting the scaling, the analytical solution, multiplied by the carrier amplitude a_0 , is then written in dimensional form, satisfying the hydrodynamic NLS equation [5]. We emphasize that the hydrodynamic time and the space NLS frameworks provide different wave profile evolutions for Akhmediev-type breathers [65]. At a specific distance, the temporal variation of envelope can be easily reconstructed from the surface measurements by use of the Hilbert transform [21].

Figure 7.6(a) shows the results of experiments carried out in the water wave tank by considering an initial localized perturbation centered at $t = 0$, and by using the parameters $R = 1.15$, $\alpha = 0.4$, $\theta_{1,2} = \pi/2$, $\mu_{1,2} = 0$. After 18 m of propagation, we clearly observe that the localized perturbation develops into a pair of quasi-Akhmediev breathers that begin to move in the opposite directions, leaving behind (i.e. at the center $t = 0$) a non-perturbed plane wave. Note that the envelope asymmetry between the two breathers has to be inserted into initial conditions in order to take into account breather propagation along the tank during the excitation. For each time series, we also calculated the envelope profile corresponding to the surface elevation of the wave trains to facilitate the comparison with the theory shown in figure 7.6(b). A good agreement is obtained for both amplitude and phase of the wave trains. Theoretical profiles were based on the calculation of the free surface elevation from breather solutions and variable ψ given by equations (7.3) and (7.5) to second order in steepness.

For the reverse process of quasi-annihilation of one pair of quasi-Akhmediev breathers, the parameters $\mu_{2,1}$ of the solution are slightly shifted due to experimental restrictions ($R = 1.15$, $\alpha = 0.4$, $\theta_{1,2} = \pi/2 + \pi$, $\mu_{2,1} = \pm 2$). We experimentally confirm, in figure 7.6(c), the quasi-annihilation dynamics of the initial pair of quasi-Akhmediev breathers into a localized perturbation centered at $t = 0$, after 31.5 m of propagation. The agreement with theoretical predictions (see figure 7.6(d)) is again excellent, thus demonstrating the existence of superregular breathers in hydrodynamics, in particular for describing modulation instability in the framework

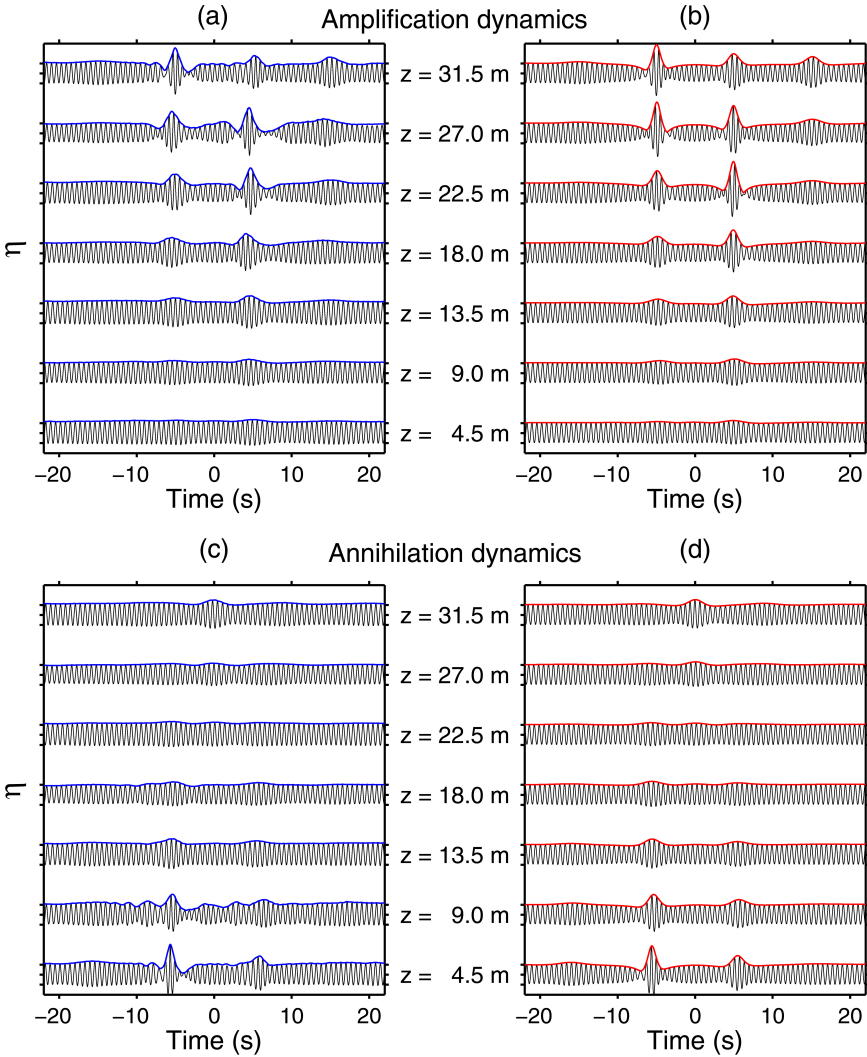


Figure 7.6. (a) and (c) Evolution of time series of surface elevation measurement as a function of propagation distance for amplification and annihilation dynamics, respectively. The surface elevation is kept in normalized units so that the amplitude of the unperturbed wave train is 1 (in dimensional units, it corresponds to 1 cm). The corresponding envelopes of the wave trains (blue lines) were calculated using the Hilbert transform. (b) and (d) Theoretical predictions of time series of surface elevation as a function of propagation distance for amplification and annihilation dynamics, respectively. The envelope of the analytical solution is shown by the red line. Adapted from [54].

of localized perturbations. Note that amplitudes are slightly lower in the experiments than theoretical prediction, for instance, due to the dissipation naturally existing when performing experiments in water wave facilities [66]. Other deviations can be also attributed to higher-order effects that cannot be captured within the standard NLS equation [67–69].

7.3.2 Light waves

For light waves, the experimental setup (see figure 7.5(b)) is mainly based on high-speed telecommunications-grade components. The ideal excitation is obtained through Fourier-transform optical pulse shaping with phase and amplitude controls of the optical field in the spectral domain. This optical processing is based on spectral line-by-line shaping of a frequency comb laser source by means of a programmable optical filter (wave shaper) in order to synthesize tailored modulated initial conditions of the continuous wave. This results in a time-periodic pattern of the perturbed continuous wave whose frequency is equal to the spectral separation of the comb lines (i.e. here equal to 20 GHz). An erbium-doped fiber amplifier is used to amplify and fix the average power of the synthesized wave according to the theoretical parameters (for each element of the periodic pattern) before coupling and propagation into 0.76 or 1.5 km long segments of the same standard single-mode optical fiber. The optical fiber exhibits anomalous group-velocity dispersion $\beta_2 = -21.1 \text{ ps}^2 \text{ km}^{-1}$, low linear losses equal to 0.2 dB km^{-1} , and a nonlinearity $\gamma = 1.2 \text{ W}^{-1} \text{ km}^{-1}$. More details about the fiber-based frequency comb source can be found in reference [38]. We then restrict the theoretical parameters to fit the limited time window over which we can inscribe arbitrary localized perturbation on the continuous wave and observe the complete nonlinear dynamics without interaction between neighboring elements of the periodic pattern. The parameters of the one-pair superregular breather solution are then adjusted, in particular $\varepsilon = 0.4$. After propagation, wave profiles are then simultaneously measured in temporal and spectral domains at the fiber output. The optical intensity profile $|A|^2$ is characterized using an ultrafast optical sampling oscilloscope with sub-picosecond resolution and a high-dynamic-range optical spectrum analyzer with 2.5 GHz resolution.

The correspondence between theory and experiment can be retrieved by recalling that dimensional distance z [m] and time t [s] are related to the previous normalized parameters by $z = \xi L_{\text{NL}}$ and $t = \tau t_0$, where the characteristic (nonlinear) length and time scales are $L_{\text{NL}} = (\gamma P_0)^{-1}$ and $t_0 = (|\beta_2| L_{\text{NL}})^{\frac{1}{2}}$, respectively [70]. The dimensional field $A(z, t)[W^{\frac{1}{2}}]$ is $A = P_0^{\frac{1}{2}}\psi$, P_0 being the average power of the perturbed continuous wave, here equal to 0.74 W. By calculating spectral (phase and intensity) profile differences between the initial frequency comb and the corresponding Fourier transform of initial condition at fiber input, one can apply the resulting (phase and intensity) corrections as a pulse-shaping mask to the wave shaper.

Figure 7.7(a) reports the development of a small localized perturbation into a pair of quasi-Akhmediev breathers measured for two propagation distances. The initial condition at the fiber input was taken from $\psi(R = 1.4, \alpha = 0.4, \theta_{1,2} = \pi/2, \mu_{2,1} = \pm 2, \xi = -1, \tau)$. By comparing with figure 7.7(b), we clearly reveal that each element of the measured periodic wave (i.e. a 50 ps time window) perfectly agrees with theory. Our experimental characterization is completed with direct spectral measurements in figure 7.7(c), since no phase information was available in the time domain. The strong spectral broadening of the initial perturbed continuous wave confirms again the nonlinear focusing of

perturbations, in agreement with theoretical predictions over a 50 dB dynamic range.

The reverse process corresponding to the quasi-annihilation of a pair of breathers into a small localized perturbation of the continuous wave was measured using the initial condition $\psi(R = 1.4, \alpha = 0.4, \theta_{1,2} = \pi/2 + \pi, \mu_{2,1} = \pm 2, \xi = -2.85, \tau)$, as shown in figure 7.7(d). Here, we evidence the quasi-annihilation dynamics after 760 m of propagation. For a longer propagation (i.e. 1500 m) we note the emergence of a single localized peak, in agreement with theory, in figure 7.7(e). This typical space-time behavior was also presented in figure 7.2(e) when looking at the reverse propagation direction. The corresponding spectral signatures are reported in figure 7.7(f). In particular, the quasi-

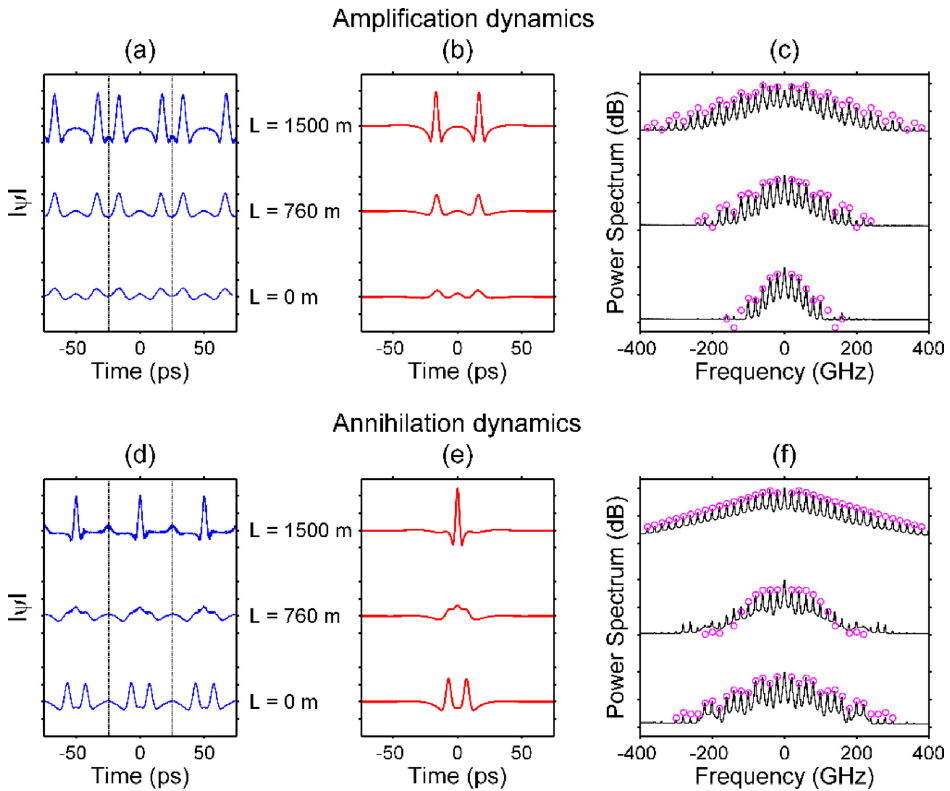


Figure 7.7. Light wave measurements for both amplification and annihilation dynamics of superregular breathers compared to theoretical predictions. Evolution of the square root of intensity profiles measured in the temporal domain as a function of propagation distance (a) and (d) and corresponding amplitude profiles from theory (b) and (e). The wave profiles are kept in normalized units so that the amplitude of the unperturbed wave train is 1. Recall that a periodic pattern of the exact solution was generated in experiments; each element of the pattern is delimited by dashed lines. (c) and (f) Comparisons of the corresponding power spectra (black solid lines for experiments, and magenta open circles for theory). Note that the theoretical spectra were sampled with the repetition rate of the experimental pattern and the delta-function component at the carrier wavelength is not shown. Adapted from [54].

annihilation stage is associated with significant spectral narrowing. The energy distributed in the multiple initial sidebands comes back to the pump and its adjacent first harmonics before being redistributed during the next nonlinear focusing.

Our experiments, which have been conducted on timescales of seconds in the water wave tank and picoseconds in the optical fiber, confirm analytical predictions of nonlinear wave theory developed recently. Demonstrating simultaneous experimental results at drastically different scales, in two different domains, are extremely rare and prove again the universal nature of MI dynamics.

7.4 Localized noise-driven modulation instability

As reported, NLS breather solutions have been generally observed following a careful control of initial excitation of the MI process. A few numerical studies have analyzed the fundamental question of how closely such analytic solutions of the NLS equation describe spontaneous emergence of localized structures in noise-driven and chaotic MI [19, 71, 72]. As suggested, some elementary and higher-order periodic breathers have been actually confirmed to exist in chaotic MI experiments [47]. A quantitative agreement can be easily obtained with numerical simulations based on the NLS equation, starting from a fully noise-perturbed plane wave. The noise perturbation is usually computed from the inverse Fourier transform of a broadband noise of one-photon per mode spectral density with random phase [71]. As a result, the characteristics of the noise-induced high-amplitude localized waves were found to cluster closely around NLS solutions. In this section, we extend the analysis to the nonlinear stage of MI emerging from time-localized noise. We address the following question: Do superregular breather solutions manifest in a genuinely chaotic and localized MI process?

In order to investigate the space-time MI dynamics excited from small localized noise, we performed simulations of MI within the framework of the NLS equation (7.1) with a locally noise-perturbed plane wave as initial condition, i.e. $\psi(\tau, \xi = 0) = 1 + \zeta(\tau)\text{sec}(\tau/\Delta)$. Here, $\zeta(\tau)$ is computed from the inverse Fourier transform of a low-amplitude broadband noise with random phase. We restrict the noise perturbation in time using a sech function with variable width Δ . Figure 7.8(a) reports the evolution map of $\psi(\tau, \xi)$ when $\Delta = 4$. We clearly observe the emergence of high-amplitude temporal peaks developing as a result of the amplification of localized noisy perturbation of the input plane wave. The MI takes place in a delimited zone of the plane (ξ, τ) , which increases with propagation distance. The edges of the MI area appear to be driven by wave structures similar to quasi-Akhmediev breathers that propagate with opposite group velocities. These velocities are partially related to the frequencies of maximum MI growth rate $\Omega_{\max} = \pm\sqrt{2}$. The corresponding spectral evolution confirms the preferential amplification of such frequencies in the initial stage of MI (i.e. $\xi < 5$), as shown in figure 7.8(c).

We can simply describe the temporal edges of MI using the one-pair superregular breather solution (see equation (7.3), with $\theta_{1,2} = \pi/2$, $\mu_{1,2} = 0$). The parameter $\alpha = \pm\pi/4$ is fixed by the value of Ω_{\max} (also defining the ‘time’ period T of quasi-

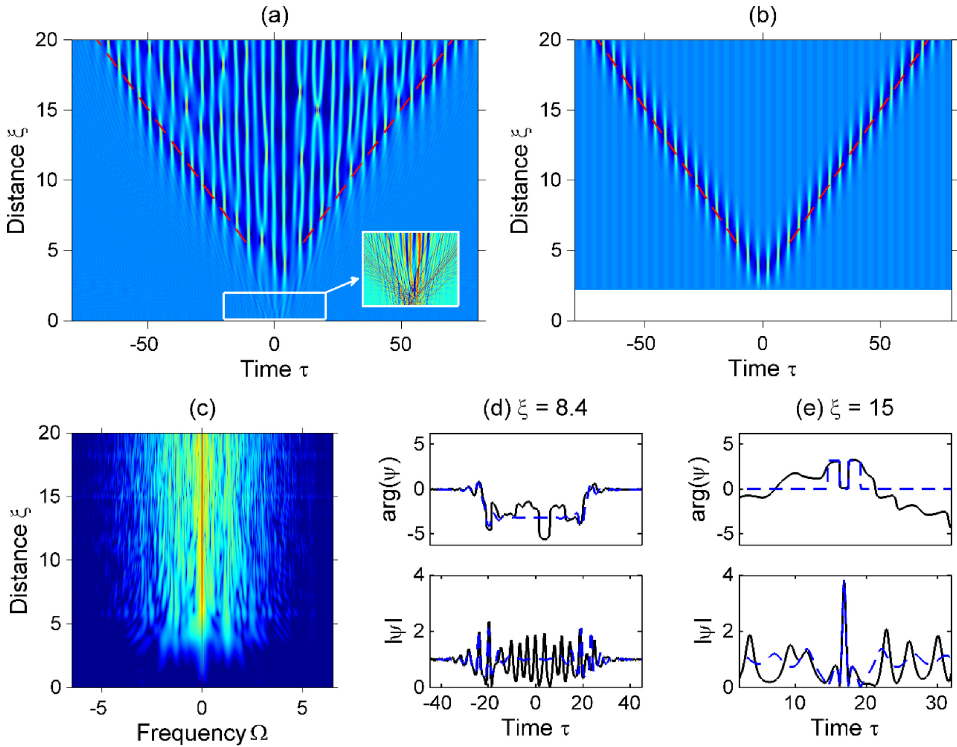


Figure 7.8. (a) NLS simulation of the temporal evolution of a small localized ($\Delta = 4$) noisy perturbation of the plane wave as a function of propagation distance. Dashed red lines indicate the temporal edges of the developing MI area. The inset (false color) zooms in on the initial transient MI stage. (b) Corresponding one-pair superregular breather solution that fits the MI edges in subfigure (a). Dashed red lines highlight opposite group velocities of the two quasi-Akhmediev breathers. (c) Spectral evolution $|\tilde{\psi}(\Omega, \xi)|$ (in log. scale) corresponding to evolution map (a). (d) Temporal profiles of both phase (top) and amplitude (bottom) obtained at $\xi = 8.4$ with NLS simulation (black lines) and breather theory (dashed blue lines), which evidence the particular properties of temporal edges of MI area. (e) Temporal phase (top) and amplitude (bottom) profiles of the highest amplitude peak detected in subfigure (a) compared to the theoretical synchronized collision of the one-pair breather solution (dashed blue lines).

Akhmediev breathers). Finally, R was adjusted to 1.2 in order to fit the absolute group velocity of MI edges highlighted in figure 7.8(a) with red dashed lines. The resulting solution is depicted in figure 7.8(b) and represents an excellent fit to the simulated MI area. Note that the origin of analytic solution was slightly shifted to $\xi_0 = 2$ to fit the numerical simulation; this depends on the energy contained in each frequency mode related to MI. Indeed, an initial transient phase (when $\xi < 2$) of MI is evidenced in the inset of figure 7.8(a), wherein a vast range of noise frequencies ($\Omega > 2$) are not amplified and then linearly dispersed from the localized perturbation. In figure 7.8(d), we confirm that temporal edges of the MI area take the form of the one-pair superregular breather solution; both amplitude and phase are well fitted by theory. Given the random initial conditions, the localized MI process cannot leave

behind (i.e. at the center $\tau = 0$) a non-perturbed plane wave exactly as the superregular breather solution. When looking at the evolution into the MI area in figure 7.8(a), the dynamics is more chaotic and we observe various forms of interaction and collision between elementary breathers similar to previous studies of noise-driven MI [71, 73]. Periodic behaviors and spatial recurrences of breather waves are clearly observable as expected. More importantly, we also demonstrate in figure 7.8(e) that the highest amplitude peak emerging at $\xi = 15$ results from the collision of two Akhmediev breathers with their particular opposite frequencies close to $\pm\Omega_{\max}$ ($R = 1$, $\alpha = 0.8$, $\theta_{1,2} = 0$, $\mu_{1,2} = 0$). The highest amplitude NLS rogue waves in the MI process are appropriately identified (amplitude and phase properties) as collisions of breathers [37].

To assess the general key role of superregular breathers in the localized MI problem, we provide additional signatures of the emergence of such complex wave structures in figure 7.9(a). The NLS evolution map of $\psi(\tau, \xi)$ for another noisy perturbation of the plane wave ($\Delta = 12$) shows again that MI takes place in a delimited zone of the plane (ξ, τ). The temporal edges of the localized MI area can be formed by a pair of quasi-Akhmediev breathers ($R = 1.07$, $\alpha = \pm\pi/4$, $\theta_{1,2} = \pi/2$, $\mu_{1,2} = 0$) that propagate with opposite group velocities, as confirmed in figure 7.9(b). Both amplitude and phase at $\xi = 11.4$ are well fitted by theory (the origin of analytic solution was shifted to $\xi_0 = 2$). Moreover, we also distinguish that another pair of quasi-Akhmediev breathers is developing into the MI area for $\xi > 7$ (see dashed white lines in figure 7.9(a)). Figure 7.9(c) depicts again both amplitude and phase profiles obtained with numerical simulation at $\xi = 11.4$, however, in this case, we are indeed able to fit some wave structures in the central zone of MI with the same one-pair superregular breather solution and its origin shifted to $\xi_0 = 6.2$. Another similar pair of quasi-Akhmediev breathers appears to emerge for $\xi \sim 12$. This spatial recurrence phenomenon can be

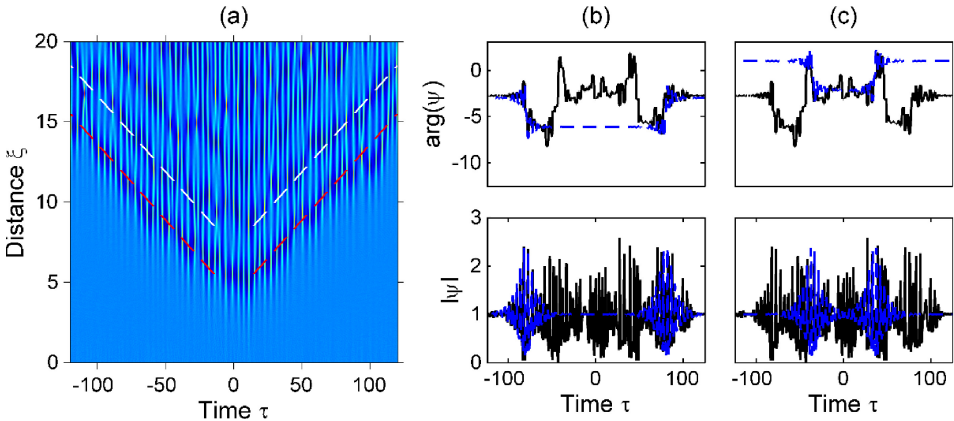


Figure 7.9. (a) NLS simulation of the temporal evolution of another small localized ($\Delta = 12$) noisy perturbation of the plane wave as a function of propagation distance. Dashed red and white lines indicate the possible position of two pairs of quasi-Akhmediev breathers in the developing MI area. (b) and (c) Corresponding temporal profiles of both phase (top) and amplitude (bottom) obtained at $\xi = 11.4$ compared with superregular breather theory (dashed blue lines).

related to the random initial conditions that are far from the exact simple perturbation described by the single one-pair superregular breather. The long-term evolution of MI dynamics from random localized perturbations still requires further studies that are beyond the scope of this chapter. Future works could also take into account the more complex theoretical framework of N -pair breather solutions.

7.5 Conclusions

This chapter reported the main physical features of NLS superregular breathers, with particular emphasis on the simplest one-pair superregular solution. We also described the first experimental evidence of such breathers in two different branches of wave physics, namely in optics and hydrodynamics. Based on the common NLS equation framework [74], the multidisciplinary approach confirmed that superregular breathers are of fundamental importance since they contribute to fully describe both amplification and annihilation stages of extreme localized waves in the modulation instability phenomenon. Here, our investigations have been restricted to an essentially reduced class of N -pair breather solutions and in the absence of complex and random dynamics. However, even the simplest one-pair breathers may describe a vast range of unstable nonlinear dynamics (for example, see figure 7.2), and contribute to solve MI-related problems such as rogue waves and turbulence in integrable systems [51, 75].

To this end, some preliminary numerical simulations were performed to analyze the localized noise-driven MI problem. These numerical results clearly highlighted that the resulting nonlinear stage of spatiotemporal MI involves the development of superregular breathers. In order to explore the rich dynamics induced by random noisy perturbation, further detailed studies are obviously still required. Note that the long-term evolution of the nonlinear stage of MI is still an open problem depending on the input perturbation considered. In particular, as was shown in references [76, 77], a broad class of modulationally unstable localized initial conditions can be described by so-called continuous spectrum solutions of the NLS equation. Besides, the impact of non-exact initial excitation of NLS breathers as well as the influence of non-ideal NLS propagation (i.e. quasi-integrable systems) are of fundamental importance to better understanding of natural phenomena and experimental systems. Any kind of disturbance of the NLS propagation induces a deviation from the theoretical breather. However, breathers may be considered as ‘robust solutions’ [78] in the sense that their main pulsating features occur even with non-ideal conditions. Note that recent efforts have been firstly made from both theoretical and experimental points of view for elementary breather solutions. For instance, breather solutions were derived of the integrable nonlinear Schrödinger equation hierarchy with an infinite number of higher-order terms [79, 80]. Approximate polynomial solutions can be also found for an extended NLS equation, taking into account higher-order odd terms or even-parity perturbations that break the integrability [81, 82]. Preliminary numerical studies recently investigated how some metamaterial properties (such as the magneto-optic effect) can affect the propagation of NLS breathers [83]. Nevertheless, experimental

characteristics are generally chosen in accordance with NLS theory requirements in order to avoid the potential impact of higher-order dispersive or nonlinear effects. Only a few experimental studies in optics and hydrodynamics reported the impact of higher-order dispersion, propagation defect or losses, or forcing on some breather dynamics and related spatial recurrence phenomena [84–88]. Finally, it is worth mentioning that major experimental developments were also achieved in the observation of breather solutions, which open new perspectives particularly in the field of experimental physics. First, recall that real-time single-shot measurements of spontaneous breathers were reported in optics from the nonlinear propagation of initially coherent or incoherent waves [47, 48]. Similar detection analysis was also confirmed in a water wave tank in which the MI process was seeded by random noise added to a Stokes wave [89]. Secondly, the evidence of polarization modulation instability and related vector breather solutions is expected to be a crucial progress in describing spontaneous wave pattern formation in multicomponent systems [90, 91].

Acknowledgments

BK acknowledges funding from the French ‘Investissements d’Avenir’ program (project PIA2/ISITE-BFC, contract ANR-15-IDEX-03) and the Conseil Régional de Bourgogne. AC acknowledges the support of the Japan Society for the Promotion of Science (JSPS). The work on theoretical breather formalism linked to hydrodynamics was supported by the Russian Science Foundation (Grant No. 14-22-00174 to AG and VZ). The work on theoretical breather formalism linked to optics was supported by the Russian Science Foundation (Grant No. 17-71-10128 to AG). NA acknowledges the support of the Australian Research Council (Discovery Project numbers DP140100265 and DP150102057) and support from the Volkswagen Stiftung.

References

- [1] Zakharov V E and Ostrovsky L A 2009 Modulation instability: The beginning *Physica D* **238** 540–8
- [2] Akhmediev N and Ankiewicz A 1997 *Solitons, Nonlinear Pulses and Beams* (London: Chapman and Hall)
- [3] Remoissenet M 2010 *Waves Called Solitons: Concepts and Experiments* (Heidelberg: Springer)
- [4] Zakharov V E and Shabat A B 1971 Exact theory of two-dimensional self-focusing and one-dimensional self-modulation of waves in nonlinear media *Zh. Eksp. Teor. Fiz.* **61** 118 [Sov. Phys. JETP **34** 62 (1972)]
- [5] Zakharov V E 1968 Stability of periodic waves of finite amplitude on a surface of deep fluid *J. Appl. Mech. Tech. Phys.* **9** 190–4
- [6] Lighthill M J 1965 Contribution to the theory of waves in non-linear dispersive systems *J. Inst. Math. Appl* **1** 269–306
- [7] Whitham G B 1965 A general approach to linear and nonlinear dispersive waves using a Lagrangian *J. Fluid Mech.* **22** 273–83
- [8] Bespalov V I and Talanov V J 1966 Filamentary structure of light beams in nonlinear liquids. *JETP Lett.* **3** 307–10

- [9] Benjamin T B and Feir J E 1967 The disintegration of wave trains on deep water. Part 1: Theory *J. Fluid Mech.* **27** 417–30
- [10] Benjamin T B 1967 Instability of periodic wavetrains in nonlinear dispersive systems *Proc. Roy. Soc. A* **299** 59–75
- [11] Taniuti T and Washimi H 1968 Self-trapping and instability of hydromagnetic waves along the magnetic field in a cold plasma *Phys. Rev. Lett.* **21** 209
- [12] Watanabe S 1977 Self-modulation of a nonlinear ion wave packet *J. Plasma Phys.* **17** 487–501
- [13] Bailung H and Nakamura Y 1993 Observation of modulational instability in a multi-component plasma with negative ions *J. Plasma Phys.* **50** 231–42
- [14] Tai K, Hasegawa A and Tomita A 1986 Observation of modulational instability in optical fibers *Phys. Rev. Lett.* **56** 135
- [15] Marquie P, Bilbault J M and Remoissenet M 1994 Generation of envelope and hole solitons in an experimental transmission line *Phys. Rev. E* **49** 828
- [16] Salasnich L, Parola A and Modulational Reatto L 2003 Instability and complex dynamics of confined matter-wave solitons *Phys. Rev. Lett.* **91** 080405
- [17] Lake B M, Yuen H C, Rungaldier H and Ferguson W E 1977 Nonlinear deep-water waves: theory and experiment. Part 2. Evolution of a continuous wave train *J. Fluid. Mech.* **83** 49–74
- [18] Akhmediev N, Ankiewicz A and Taki M 2009 Waves that appear from nowhere and disappear without a trace *Phys. Lett. A* **373** 675–8
- [19] Akhmediev N, Soto-Crespo J M and Ankiewicz A 2009 Extreme waves that appear from nowhere: On the nature of rogue waves *Phys. Lett. A* **373** 2137–45
- [20] Kharif C, Pelinovsky E and Slunyaev A 2009 *Rogue Waves in the Ocean* (Berlin–Heidelberg: Springer)
- [21] Osborne A R 2010 *Nonlinear Ocean Waves and the Inverse Scattering Transform* (San Diego: Academic)
- [22] Kuznetsov E 1977 Solitons in a parametrically unstable plasma *Sov. Phys. Dokl* **22** 507–8
- [23] Kawata T and Inoue H 1978 Inverse scattering method for the nonlinear evolution equations under nonvanishing conditions *J. Phys. Soc. Jpn* **44** 1722–9
- [24] Ma Y C 1979 The perturbed plane-wave solutions of the cubic Schrödinger equation *Stud. Appl. Math.* **60** 43–58
- [25] Peregrine D H 1983 Water waves, nonlinear Schrödinger equations and their solutions *J. Austral. Math. Soc. Ser. B* **25** 16–43
- [26] Akhmediev N and Korneev V I 1986 Modulation instability and periodic solutions of the nonlinear Schrödinger equation *Theor. Math. Phys.* **69** 1089–93
- [27] Akhmediev N, Eleonskii V M and Kulagin N E 1987 Exact first-order solutions of the nonlinear Schrödinger equation *Theor. Math. Phys.* **72** 809–18
- [28] Kedziora D J, Ankiewicz A and Akhmediev N 2013 Classifying the hierarchy of nonlinear-Schrödinger-equation rogue-wave solutions *Phys. Rev. E* **88** 013207
- [29] Kibler B, Fatome J, Finot C, Millot G, Dias F, Genty G, Akhmediev N and Dudley J M 2010 The Peregrine soliton in nonlinear fibre optics *Nat. Phys.* **6** 790–5
- [30] Hammani K, Wetzel B, Kibler B, Fatome J, Finot C, Millot G, Akhmediev N and Dudley J M 2011 The spectral dynamics of modulation instability described using Akhmediev breather theory *Opt. Lett.* **36** 2140–2
- [31] Chabchoub A, Hoffmann N P and Akhmediev N 2011 Rogue wave observation in a water wave tank *Phys. Rev. Lett.* **106** 204502

- [32] Bailung H, Sharma S K and Nakamura Y 2011 Observation of Peregrine solitons in a multicomponent plasma with negative ions *Phys. Rev. Lett.* **107** 255005
- [33] Erkintalo M, Hammani K, Kibler B, Finot C, Akhmediev N, Dudley J M and Genty G 2011 Higher order modulation instability in nonlinear fiber optics *Phys. Rev. Lett.* **107** 253901
- [34] Chabchoub A, Hoffmann N, Onorato M and Akhmediev N 2012 Super rogue waves: observation of a higher-order breather in water waves *Phys. Rev. X* **2** 011015
- [35] Chabchoub A, Neumann S, Hoffmann N P and Akhmediev N 2012 Spectral properties of the Peregrine soliton observed in a water wave tank *J. Geophys. Res.* **117** C00J02
- [36] Chabchoub A and Akhmediev N 2013 Observation of rogue wave triplets in water waves *Phys. Lett. A* **377** 2590–3
- [37] Frisquet B, Kibler B and Millot G 2013 Collision of Akhmediev breathers in nonlinear fiber optics *Phys. Rev. X* **3** 041032
- [38] Frisquet B, Chabchoub A, Fatome J, Finot C, Kibler B and Millot G 2014 Two-stage linear-nonlinear shaping of an optical frequency comb as rogue nonlinear-Schrödinger-equation-solution generator *Phys. Rev. A* **89** 023821
- [39] Chabchoub A, Kibler B, Dudley J M and Akhmediev N 2014 Hydrodynamics of periodic breathers *Phil. Trans. R. Soc. A* **372** 20140005
- [40] Pallabi P, Sharma S K, Nakamura Y and Bailung H 2016 Observation of second order ion acoustic Peregrine breather in multicomponent plasma with negative ions *Phys. Plasmas* **23** 022107
- [41] Chabchoub A, Waseda T, Kibler B and Akhmediev N 2017 Experiments on higher-order and degenerate akhmediev breather-type rogue water waves *J. Ocean Eng. Mar. Energy* **3** 385–94
- [42] Akhmediev N, Kibler B and Baronio F *et al* 2016 Roadmap on optical rogue waves and extreme events *J. Opt.* **18** 063001
- [43] Chabchoub A 2016 Tracking breather dynamics in irregular sea state conditions *Phys. Rev. Lett.* **117** 144103
- [44] Calini A and Schober C M 2002 Homoclinic chaos increases the likelihood of rogue wave formation *Phys. Lett. A* **298** 335–49
- [45] Onorato M 2003 Landau damping and coherent structures in narrow-banded 1 + 1 deep water gravity waves *Phys. Rev. E* **67** 046305
- [46] Kibler B, Hammani K, Michel C, Finot C and Picozzi A 2011 Rogue waves, rational solitons and wave turbulence theory *Phys. Lett. A* **375** 3149–55
- [47] Närhi M, Wetzel B, Billet C, Toenger S, Sylvestre T, Merolla J-M, Morandotti R, Dias F, Genty G and Dudley J M 2016 Real-time measurements of spontaneous breathers and rogue wave events in optical fibre modulation instability *Nat. Commun.* **7** 13675
- [48] Suret P, El Koussaifi R, Tikan A, Evain C, Randoux S, Szwej C and Bielawski S 2016 Single-shot observation of optical rogue waves in integrable turbulence using time microscopy *Nat. Commun.* **7** 13136
- [49] Zakharov V E 2009 Turbulence in Integrable Systems *Stud. Appl. Math.* **122** 219–34
- [50] Agafontsev D S and Zakharov V E 2015 Integrable turbulence and formation of rogue waves *Nonlinearity* **28** 2791–821
- [51] Soto-Crespo J M, Devine N and Akhmediev N 2016 Integrable turbulence and rogue waves: breathers or solitons? *Phys. Rev. Lett.* **116** 103901
- [52] Zakharov V E and Gelash A A 2013 Nonlinear stage of modulation instability *Phys. Rev. Lett.* **111** 054101

- [53] Gelash A A and Zakharov V E 2014 Superregular solitonic solutions: a novel scenario for the nonlinear stage of modulation instability *Nonlinearity* **27** R1–39
- [54] Kibler B, Chabchoub A, Gelash A A, Akhmediev N and Zakharov V E 2015 Superregular breathers in optics and hydrodynamics: omnipresent modulation instability beyond simple periodicity *Phys. Rev. X* **5** 041026
- [55] Zhang J-H, Wang L and Liu C 2017 Superregular breathers, characteristics of nonlinear stage of modulation instability induced by higher-order effects *Proc. R. Soc. A* **473** 20160681
- [56] Liu C, Ren Y, Yang Z Y and Yang W L 2017 Superregular breathers in a complex modified Korteweg-de Vries system *Chaos* **27** 083120
- [57] Zakharov V E and Shabat A B 1979 Integration of nonlinear equations of mathematical physics by the method of inverse scattering II *Funct. Anal. Appl.* **13** 166–74
- [58] Faddeev L D and Takhtajan L A 2007 *Hamiltonian Methods in the Theory of Solitons* (Heidelberg: Springer)
- [59] Tajiri M and Watanabe Y 1998 Breather solutions to the focusing nonlinear Schrödinger equation *Phys. Rev. E* **57** 3510
- [60] Akhmediev N, Ankiewicz A and Soto-Crespo J M 2009 Rogue waves and rational solutions of the nonlinear Schrödinger equation *Phys. Rev. E* **80** 026601
- [61] Akhmediev N, Soto-Crespo J M and Ankiewicz A 2009 How to excite a rogue wave *Phys. Rev. A* **80** 043818
- [62] Kibler B, Fatome J, Finot C, Millot G, Genty G, Wetzel B, Akhmediev N, Dias F and Dudley J M 2012 Observation of Kuznetsov–Ma soliton dynamics in optical fibre *Sci. Rep.* **2** 463
- [63] Akhmediev N, Ankiewicz A, Soto-Crespo J M and Dudley J M 2011 Universal triangular spectra in parametrically-driven systems *Phys. Lett. A* **375** 775–9
- [64] Devine N, Ankiewicz A, Genty G, Dudley J M and Akhmediev N 2011 Recurrence phase shift in Fermi–Pasta–Ulam nonlinear dynamics *Phys. Lett. A* **375** 4158–61
- [65] Chabchoub A and Grimshaw R H J 2016 The hydrodynamic nonlinear Schrödinger equation: Space and time *Fluids* **1** 23
- [66] Henderson D M and Segur H 2013 The role of dissipation in the evolution of ocean swell *J. Geophys. Res.* **118** 5074–91
- [67] Dysthe K B 1979 Note on the modification of the nonlinear Schrödinger equation for application to deep water waves *Proc. R. Soc. A* **369** 105–14
- [68] Trulsen K and Dysthe K B 1996 A modified nonlinear Schrödinger for broader bandwidth gravity waves on deep water *Wave Motion* **24** 281–9
- [69] Craig W, Guyenne P and Sulem C 2010 Hamiltonian approach to nonlinear modulation of surface water waves *Wave Motion* **47** 552–63
- [70] Agrawal G P 2013 *Nonlinear Fiber Optics* 5th edition (Oxford: Academic)
- [71] Toenger S, Godin T, Billet C, Dias F, Erkintalo M, Genty G and Dudley J M 2015 Emergent rogue wave structures and statistics in spontaneous modulation instability *Sci. Rep.* **5** 10380
- [72] Agafontsev D S and Zakharov V E 2016 Integrable turbulence generated from modulational instability of cnoidal waves *Nonlinearity* **29** 3551–78
- [73] Dudley J M, Genty G, Dias F, Kibler B and Akhmediev N 2009 Modulation instability, Akhmediev breathers and continuous wave supercontinuum generation *Opt. Exp.* **17** 21497–508

- [74] Chabchoub A, Kibler B, Finot C, Millot G, Onorato M, Dudley J M and Babanin A V 2015 The nonlinear Schrödinger equation and the propagation of weakly nonlinear waves in optical fibers and on the water surface *Ann. Phys.* **361** 490–500
- [75] Akhmediev N, Soto-Crespo J M and Devine N 2016 Breather turbulence versus soliton turbulence: Rogue waves, probability density functions, and spectral features *Phys. Rev. E* **94** 022212
- [76] Biondini G and Mantzavinos D 2016 Universal nature of the nonlinear stage of modulational instability *Phys. Rev. Lett.* **116** 043902
- [77] Biondini G, Li S and Mantzavinos D 2016 Oscillation structure of localized perturbations in modulationally unstable media *Phys. Rev. E* **94** 060201
- [78] Ankiewicz A, Devine N and Akhmediev N 2009 Are rogue waves robust against perturbations? *Phys. Lett. A* **373** 3997–4000
- [79] Ankiewicz A, Kedziora D J, Chowdhury A, Bandelow U and Akhmediev N 2016 Infinite hierarchy of nonlinear Schrödinger equations and their solutions *Phys. Rev. E* **93** 012206
- [80] Ankiewicz A and Akhmediev N 2017 Rogue wave solutions for the infinite integrable nonlinear Schrödinger equation hierarchy *Phys. Rev. E* **96** 012219
- [81] Ankiewicz A, Soto-Crespo J M, Chowdhury M A and Akhmediev N 2013 Rogue waves in optical fibers in presence of third-order dispersion, self-steepening, and self-frequency shift *J. Opt. Soc. Am. B* **30** 87–94
- [82] Ankiewicz A, Chowdhury A, Devine N and Akhmediev N 2013 Rogue waves of the nonlinear Schrödinger equation with even symmetric perturbations *J. Opt.* **15** 064007
- [83] Boardman A, Alberucci A, Assanto G, Grimalsky V, Kibler B, McNiff J, Nefedov I, Rapoport Y and Valagiannopoulos C 2017 Waves in hyperbolic and double negative metamaterials including rogues and solitons *Nanotechnology* **28** 444001
- [84] Chabchoub A, Hoffmann N, Branger H, Kharif C and Akhmediev N 2013 Experiments on wind-perturbed rogue wave hydrodynamics using the Peregrine breather model *Phys. Fluids* **25** 101704
- [85] Mussot A, Kudlinski A, Droques M, Szriftgiser P and Akhmediev N 2014 Fermi–Pasta–Ulam recurrence in nonlinear fiber optics: The role of reversible and irreversible losses *Phys. Rev. X* **4** 011054
- [86] Kimmoun O *et al* 2016 Modulation instability and phase-shifted Fermi–Pasta–Ulam recurrence *Sci. Rep.* **6** 28516
- [87] Kimmoun O, Hsu H C, Kibler B and Chabchoub A 2017 Non-conservative higher-order hydrodynamic modulation instability *Phys. Rev. E* **96** 022219
- [88] Bendahmane A, Mussot A, Szriftgiser P, Zerkak O, Genty G, Dudley J M and Kudlinski A 2014 Experimental dynamics of Akhmediev breathers in a dispersion varying optical fiber *Opt. Lett.* **39** 4490–3
- [89] Chabchoub A, Genty G, Dudley J M, Kibler B and Waseda T 2017 Experiments on spontaneous modulation instability in hydrodynamics *27th Int. Ocean and Polar Engineering Con. (ISOPE-2017)*
- [90] Frisquet B, Kibler B, Morin P, Baronio F, Conforti M, Millot G and Wabnitz S 2016 Optical dark rogue wave *Sci. Rep.* **6** 20785
- [91] Frisquet B, Kibler B, Fatome F, Morin P, Baronio F, Conforti M, Millot G and Wabnitz S 2015 Polarization modulation instability in a Manakov fiber system *Phys. Rev. A* **92** 053854